Plasmonic effects of quantum size metal nanoparticles on dye-sensitized solar cell

N.B. When citing this work, cite the original published paper.

(article starts on next page)

Plasmonic effects of quantum size metal nanoparticles on dye-sensitized solar cell

S. SHAH,[1] I. M. NOOR,[1] J. PITAWALA,[2] I. ALBINSON,[3] T. M. W. J. BANDARA,[4,5] B. -E. MELLANDER,[5] AND A. K. AROF[1,*]

[1]Centre for Ionics University of Malaya, Department of Physics, University of Malaya, 50603 Kuala Lumpur, Malaysia
[2]Department of Science and Technology, Uva Wellassa University, Badulla, Sri Lanka
[3]Department of Physics, University of Gothenburg, Gothenburg, Sweden
[4]Department of Physical Sciences, Rajarata University of Sri Lanka, Mihintale, Sri Lanka
[5]Department of Physics, Chalmers University of Technology, Gothenburg, Sweden
*akarof@um.edu.my

Abstract: Gel polymer electrolytes (GPEs) based on poly(ethylene oxide) (PEO) and phthaloyl chitosan (PhCh) for dye-sensitized solar cells (DSSCs) have been synthesized and characterized. The GPEs have been prepared using different weight fractions of PEO and PhCh that have been added to a fixed composition solution of tetrapropylammonium iodide (TPAI), dimethylformamide (DMF) and iodine (I_2) crystals. The ionic conductivity behavior of prepared GPEs was studied using impedance spectroscopy. The sample having 70 wt.% PEO and 30 wt.% PhCh showed the highest ionic conductivity of 7.36 mS cm^{-1} at room temperature. The photoanode of the DSSC consists of two TiO_2 layers. The first or compact layer has a thickness of ~5 μm and the TiO_2 nanoparticles have an average size of 14 nm. The second layer of TiO_2 nanoparticles has an average size of 21 nm. In order to adsorb dye molecules, the TiO_2 photoanodes were soaked in anthocyanin and ruthenium 535 (N3) dye solutions. The GPE has been deposited between the dye/TiO_2 photoanode and platinum (Pt) counter electrode in a sandwich-like structure. Results showed that the fabricated DSSC with an electrolyte containing 70 wt.% PEO:30 wt.% PhCh exhibited the highest efficiency for both anthocyanin and N3 dyes and the efficiency and ionic conductivity trend versus PEO content are similar. On addition of different amounts of Ag nanoparticles (0, 10, 20, 30, 40 μL), with average size of 10 nm to the second TiO_2 layer, the performance of DSSCs with anthocyanin sensitizer and N3 dye improved. The cell with anthocyanin/(TiO_2 + 10 μL Ag nanoparticles) showed a 21%, 17.2% and 39.6% increase in short circuit current density (J_{sc}), fill factor *(FF)*, and light to electricity conversion efficiency (η) respectively compared to the cell without Ag nanoparticle. The DSSC fabricated with TiO_2 photoanode containing 20 μL Ag nanoparticles soaked in N3 dye exhibits J_{sc}, *FF*, and η of 15.24 mA cm^{-2}, 57% and 5.21% respectively. The incorporation of Ag nanoparticles has resulted in a 17% and 13% increase in J_{sc}, and η, respectively, for N3 based cells. This performance enhancement with the addition of Ag nanoparticles can be attributed to improvement of light scattering and charge transport as a result of plasmonic resonance.

References and links

1. F. Bella, and R. Bongiovanni, "Photoinduced polymerization: An innovative, powerful and environmentally friendly technique for the preparation of polymer electrolytes for dye-sensitized solar cells," J. Photochem. Photobiol. Chem. **16**, 1–21 (2013).
2. N. S. Lewis, "Toward cost-effective solar energy use," Science **315**(5813), 798–801 (2007).
3. Q. Zhang and G. Cao, "Nanostructured photoelectrodes for dyesensitized solar cells," Nano Today **6**(1), 91–109 (2011).
4 D. Eli, M.S. Ahmad, A.B. Bikimi, and O.A. Babatunde, "Plasmonic dye sensitized solar cells incorporated with TiO_2-Ag nanostructures," International Research Journal of Pure and Applied Chemistry **11**(3), 1–7 (2016).

5. M. Grätzel, "Dye-sensitized solar cells," J. Photochem. Photobiol. Chem. **4**(2), 145–153 (2003).
6. M. A. Green, K. Emery, Y. Hishikawa, and W. Warta, "Solar cell efficiency tables (version 33)," Prog. Photovolt. Res. Appl. **17**(5), 320–326 (2009).
7. K. Yoo, J. Y. Kim, J. A. Lee, J. S. Kim, D. K. Lee, K. Kim, J. Y. Kim, B. Kim, H. Kim, W. M. Kim, J. H. Kim, and M. J. Ko, "Completely transparent conducting oxide-free and flexible dye-sensitized solar cells fabricated on plastic substrates," ACS Nano **9**(4), 3760–3771 (2015).
8. K. M. Lee, L. C. Lin, C. Y. Chen, V. Suryanarayanan, and C. G. Wu, "Preparation of high transmittance platinum counter electrode at an ambient temperature for flexible dye-sensitized solar cells," Electrochim. Acta **135**, 578–584 (2014).
9. T. M. W. J. Bandara, W. J. M. J. S. R. Jayasundara, H. D. N. S. Fernado, M. A. K. L. Dissanayake, L. A. A. De Silva, I. Albinsson, M. Furlani, and B.-E. Mellander, "Efficiency of 10% for quasi-solid state dye-sensitized solar cells under low light irradiance," J. Appl. Electrochem. **45**(4), 289–298 (2015).
10. L. Wang, H. Zhang, C. Wang, and T. Ma, "Highly stable gel-state dye-sensitized solar cells based on high soluble polyvinyl acetate," ACS Sustain. Chem.& Eng. **1**(2), 205–208 (2013).
11. X. Zhang, H. Yang, H. M. Xiong, F. Y. Li, and Y. Y. Xia, "A quasi-solid-state dye-sensitized solar cell based on the stable polymer-grafted nanoparticle composite electrolyte," J. Power Sources **160**(2), 1451–1455 (2006).
12. Z. Lan, J. Wu, D. Wang, S. Hao, J. Lin, and Y. Huang, "Quasi-solid state dye-sensitized solar cells based on gel polymer electrolyte with poly (acrylonitrile-co-styrene)/NaI+ I$_2$," Sol. Energy **80**(11), 1483–1488 (2006).
13. J. Wu, Z. Lan, J. Lin, M. Huang, Y. Huang, L. Fan, and G. Luo, "Electrolytes in dye-sensitized solar cells," Chem. Rev. **115**(5), 2136–2173 (2015).
14. M. S. Su'ait, M. Y. A. Rahman, and A. Ahmad, "Review on polymer electrolyte in dye-sensitized solar cells (DSSCs)," Sol. Energy **115**, 452–470 (2015).
15. H. Yang, M. Huang, J. Wu, Z. Lan, S. Hao, and J. Lin, "The polymer gel electrolyte based on poly (methyl methacrylate) and its application in quasi-solid-state dye-sensitized solar cells," Mater. Chem. Phys. **110**(1), 38–42 (2008).
16. D. W. Kim, Y. B. Jeong, S. H. Kim, D. Y. Lee, and J. S. Song, "Photovoltaic performance of dye-sensitized solar cell assembled with gel polymer electrolyte," J. Power Sources **149**, 112–116 (2005).
17. T. M. W. J. Bandara, H. D. N. S. Fernando, M. Furlani, I. Albinsson, M. A. K. L. Dissanayake, and B.-E. Mellander, "Performance enhancers for gel polymer electrolytes based on LiI and RbI for quasi-solid-state dye sensitized solar cells," RSC Advances **6**(105), 103683 (2016).
18. T. M. W. J. Bandara, T. Svensson, M. A. K. L. Dissanayake, M. Furlani, W. J. M. J. S. R. Jayasundara, and B.-E. Mellander, "Tetrahexylammonium iodide containing solid and gel polymer electrolytes for dye sensitized solar cells," Energy Procedia **14**, 1607–1612 (2012).
19. Y. Ren, Z. Zhang, S. Fang, M. Yang, and S. Cai, "Application of PEO based gel network polymer electrolytes in dye-sensitized photoelectrochemical cells," Sol. Energy Mater. Sol. Cells **71**(2), 253–259 (2002).
20 S.N.F. Yusuf, M.F. Aziz, H.C. Hassan, T.M.W.J. Bandara, B.-E. Mellander, M.A. Careem, A.K. Arof, "Phthaloylchitosan-Based Gel Polymer Electrolytes for Efficient Dye-Sensitized Solar Cells," J. Chem. **2014**, 783023 (2014).
21. A. K. Arof, M. F. Aziz, M. M. Noor, M. A. Careem, L. R. A. K. Bandara, C. A. Thotawatthage, W. N. S. Rupasinghe, and M. A. K. L. Dissanayake, "Efficiency enhancement by mixed cation effect in dye-sensitized solar cells with a PVdF based gel polymer electrolyte," Int. J. Hydrogen Energy **39**(6), 2929–2935 (2014).
22. J. Wu, Z. Lan, J. Lin, M. Huang, Y. Huang, L. Fan, and G. Luo, "Electrolytes in dye-sensitized solar cells," Chem. Rev. **115**(5), 2136–2173 (2015).
23. A. M. Stephan, "Review on gel polymer electrolytes for lithium batteries," Eur. Polym. J. **42**(1), 21–42 (2006).
24. A. M. Stephan, and K. S. Nahm, "Review on composite polymer electrolytes for lithium batteries," Polymer (Guildf.) **47**(16), 5952–5964 (2006).
25. C. Sequeira, and D. Santos, *Polymer Electrolytes: Fundamentals and Applications* (Elsevier, Woodhead Publishing, 2010).
26. N. A. Ludin, A. A. A. Mahmoud, A. B. Mohamad, A. A. H. Kadhum, K. Sopian, and N. S. A. Karim, "Review on the development of natural dye photosensitizer for dye-sensitized solar cells," J. Renew. Sustain. Energ. **31**, 386–396 (2014).
27. L. L. Li and E. W. G. Diau, "Porphyrin-sensitized solar cells," Chem. Soc. Rev. **42**(1), 291–304 (2013).
28. Y. Qin, and Q. Peng, "Ruthenium sensitizers and their applications in dye-sensitized solar cells," Int. J. Photoenergy **2012**(291579), 1–21 (2012).
29. P. Mandal, and S. Sharma, "Progress in plasmonic solar cell efficiency improvement: A status review," J. Renew. Sustain. Energ. **65**, 537–552 (2016).
30. T. M. Chien, P. Pavaskar, W. H. Hung, S. Cronin, S. H. Chiu, and S. N. Lai, "Study of the plasmon energy transfer processes in dye sensitized solar cells," J. Nanomater. **2015**, 2 (2015).
31. Y. H. Jang, Y. J. Jang, S. T. Kochuveedu, M. Byun, Z. Lin, and D. H. Kim, "Plasmonic dye-sensitized solar cells incorporated with Au-TiO$_2$ nanostructures with tailored configurations," Nanoscale **6**(3), 1823–1832 (2014).
32. T. C. Wen, and W. C. Chen, "Blending thermoplastic polyurethanes and poly(ethylene oxide) for composite electrolytes via a mixture design approach," J. Appl. Polym. Sci. **77**(3), 680–692 (2000).
33. D. R. Paul, *Polymer Blends, Vol. 1* (Elsevier, 2012).

34. I. Nicotera, L. Coppola, C. Oliviero, M. Castriota, and E. Cazzanelli, "Investigation of ionic conduction and mechanical properties of PMMA–PVdF blend-based polymer electrolytes," Solid State Ion. **177**(5), 581–588 (2006).
35. G. Richhariya, A. Kumar, P. Tekasakul, and B. Gupta, "Natural dyes for dye sensitized solar cell: A review," J. Renew. Sustain. Energ. **69**, 705–718 (2017).
36 Y. Qin, and Q. Peng, "Ruthenium sensitizers and their applications in dye-sensitized solar cells," Int. J. Photoenergy **2012**, 291579 (2012).
37. Y. Wu, M. Marszalek, S. M. Zakeeruddin, Q. Zhang, H. Tian, M. Grätzel, and W. Zhu, "High-conversion-efficiency organic dye-sensitized solar cells: molecular engineering on D–A–π-A featured organic indoline dyes," Energy Environ. Sci. **5**(8), 8261–8272 (2012).
38. S. Sarker, A. J. S. Ahammad, H. W. Seo, and D. M. Kim, "Electrochemical impedance spectra of dye-sensitized solar cells: fundamentals and spreadsheet calculation," Int. J. Photoenergy **2012**, 851705 (2014).
39. A. K. Arof, S. Amirudin, S. Z. Yusof, and I. M. Noor, "A method based on impedance spectroscopy to determine transport properties of polymer electrolytes," Phys. Chem. Chem. Phys. **16**(5), 1856–1867 (2014).
40. S. P. Lim, A. Pandikumar, N. M. Huang, H. N. Lim, G. Gu, and T. L. Ma, "Promotional effect of silver nanoparticles on the performance of N-doped TiO_2 photoanode-based dye-sensitized solar cells," RSC Advances **4**(89), 48236–48244 (2014).
41. S. P. Lim, A. Pandikumar, N. M. Huang, and H. N. Lim, "Enhanced photovoltaic performance of silver @ titania plasmonic photoanode in dye-sensitized solar cells," RSC Advances **4**(72), 38111–38118 (2014).
42. B. Yu, K. M. Leung, Q. Guo, W. M. Lau, and J. Yang, "Synthesis of $Ag-TiO_2$ composite nano thin film for antimicrobial application," Nanotechnology **22**(11), 115603 (2011).
43. R.-Y. Yang, H.-Y. Chen, and F.-D. Lai, "Performance Degradation of Dye-Sensitized Solar Cells Induced by Electrolytes," Adv. Mater. Sci. Eng. **2012**, 4 (2012).
44. N. Ghobadi, "Band gap determination using absorption spectrum fitting procedure," Int. Nano Lett. **3**(1), 2 (2013).
45. L. Wei, X. Xia, Y. Yang, P. Wang, Y. Dong, and T. Luan, "Variable temperature spectroelectrochemistry study of silver-doped TiO_2 and its influence on the performance of dye sensitized solar cells," RSC Advances **6**(72), 68341–68350 (2016).
46. H. F. Zarick, O. Hurd, J. A. Webb, C. Hungerford, W. R. Erwin, and R. Bardhan, "Enhanced Efficiency in Dye-Sensitized Solar Cells with Shape-Controlled Plasmonic Nanostructures," ACS Photonics **1**(9), 806–811 (2014).
47. J. Qi, X. Dang, P. T. Hammond, and A. M. Belcher, "Highly efficient plasmon-enhanced dye-sensitized solar cells through metal@oxide core-shell nanostructure," ACS Nano **5**(9), 7108–7116 (2011).
48. N. J. Halas, S. Lal, W. S. Chang, S. Link, and P. Nordlander, "Plasmons in strongly coupled metallic nanostructures," Chem. Rev. **111**(6), 3913–3961 (2011).

1. Introduction

Annually earth receives a huge amount of light energy from the sun [1,2] and the use of this energy to satisfy our energy requirements is urgent due to several reasons. This include the inevitable exhaustion of fossil fuel in the coming fifty years [3] and the environmental damage caused by the combustion of large amounts of fossil fuels. Therefore, conversion of solar energy into a most usable form i.e. electrical energy is highly important to fulfill the ever increasing demand for energy. In addition, solar cells are environmental friendly devices and the sun is a potential energy resource. Harvesting the light energy reaching earth in an eco-friendly way can solve many issues associated with both the energy demand and global environment [4]. Research activities on solar energy conversion have been gaining more attention during the last decade.

The conversion of solar energy into electricity is done by photovoltaic devices. So far photovoltaics have undergone three generations. The first generation is silicon solar cells and the second generation is based on semiconductor thin films [4]. Dye-sensitized solar cells (DSSCs) and organic semiconductor solar cells represent the third generation of photovoltaic devices [5]. Compared to the first and second generation solar cells, the energy conversion efficiency and stability of third generation solar cells are low [6]. However, the third generation solar cells have many advantages over their first and second generation counterparts that led to attract worldwide research interest. For instance, DSSCs are flexible in shape and design, low-cost and easy to manufacture, colored, transparent, are able to performed under diffuse light condition and have low material costs [5, 7–9].

Many of the instability issues in DSSCs originate from the liquid electrolytes in these devices. This issue can be overcome by replacing the liquid electrolytes in DSSCs with gel polymer electrolytes (GPEs). Although DSSCs based on volatile liquid electrolytes ensure

higher energy conversion efficiency, they are associated with disadvantages such as risk of solvent evaporation, instability, flammability at high temperatures and dye degradation and desorption [10–12]. Quasi solid-state or gel polymer electrolytes can address some of the instability issues associated with liquid electrolytes [13,14]. For such cells, a gel-type membrane is obtained by entrapping liquid solvents/salt mixtures in a polymeric matrix. The polymers generally used for these systems are poly(methyl methacrylate) (PMMA) [15,16], poly(acrylonitrile) (PAN) [17,18], poly(ethylene oxide) (PEO) [19], phthaloyl chitosan (PhCh) [20] and poly(vinylidene fluoride) (PVdF) [21]. Several efforts have been made so far to increase the conductivity in polymer based quasi-solid electrolyte. Popular methods are to use plasticizers and/or inorganic fillers like titania, silica or alumina [22–24]. The nature and the concentration of ionic species in the electrolyte also have a profound influence on the conductivity in these polymer electrolytes [25]. However, in this work PhCh and PEO were mixed to prepare a stable and highly conductive GPE for DSSCs.

The other main problem associated with DSSCs is the low energy conversion efficiency. In DSSCs, light harvesting or photon capturing is done by dye molecules, whereas wide-bandgap semiconductor (for example TiO_2) facilitates charge separation. Several research works have been done on increasing the extinction coefficient and broadening the spectral absorption window [26–28]. However, it was reported recently that the photon absorption in DSSCs can be enhanced by scattering them with metal nanoparticles in order to enhance the overall energy conversion efficiency [29]. The efficiency enhancement in such cells can be attributed to surface plasmon resonance induced by nanoparticles [30, 31]. In the present work, we also focused to enhance the efficiency of quasi solid-state solar cells based on dye sensitizers anthocyanin and N3 (cis-Bis(isothiocyanato) bis(2,2'-bipyridyl-4,4'-dicarboxylato ruthenium(II)), respectively by adding different amounts of Ag nanoparticles in the second layer mesoporous TiO_2 photoanode.

2. Experimental

2.1 Gel polymer electrolyte preparation

In preparing gel polymer electrolytes (GPEs), 0.164 g of tetrapropylammonium iodide (TPAI) obtained from Sigma Aldrich was first dissolved in 0.89 g dimethylformamide (DMF) (Sigma Aldrich) in a glass container and stirred for 1 h. Corresponding amounts of PhCh and PEO (procured from Sigma Aldrich) as listed in Table 1 were then added to the salt solution and stirred continuously at 353 K until a homogenous mixture was obtained. Heating was then stopped and iodine (I_2) crystals (10 mole% of TPAI salt used) was added into the GPEs. Stirring was continued until the GPEs have cooled down to room temperature (298K).

Table 1. Designation and sample composition of gel polymer electrolytes.

Designation	PhCh:PEO (wt. %: wt.%)	PhCh (g)	PEO (g)	TPAI (g)	DMF (g)	I_2 (g)
S1	50:50	0.10	0.10	0.164	0.89	0.0286
S2	40:60	0.08	0.12	0.164	0.89	0.0286
S3	30:70	0.06	0.14	0.164	0.89	0.0286
S4	20:80	0.04	0.16	0.164	0.89	0.0286
S5	10:90	0.02	0.18	0.164	0.89	0.0286

2.2 Ionic conductivity measurement of GPEs

The GPE was filled in a coin cell and then sandwiched between two stainless steel electrodes. The electrodes were connected to the HIOKI LCR Hi-Tester and the impedance data ware measured in a frequency range between 50 Hz and 5 MHz at room temperature (298 K). From the plot of real and imaginary parts of the impedance, the bulk resistance (R_b) of electrolyte was determined and the conductivity (σ) was calculated using the following equation:

$$\sigma = \frac{t}{R_b A} \tag{1}$$

Here t is the thickness of the gel electrolyte sample and A is the surface area of the electrolyte.

2.3 TiO₂ electrode preparation

Photoanode with two TiO_2 layers was prepared in this work. The first TiO_2 layer is a compact layer while the second TiO_2 layer is a mesoporous layer. In the preparation of the first TiO_2 layer of ~5 μm thickness, 0.5 g of TiO_2 (Degussa P90), powder of average size 14 nm and 2.5 mL of HNO_3 (pH = 1) was ground in a mortar for 30 min. A drop of this homogenous slurry was then spin coated on the well cleaned FTO glass at 2350 rpm for 60 s. The coated glass was sintered at 723 K for 30 min and then allowed to cool to room temperature. The second TiO_2 layer was coated on the first TiO_2 layer. In the preparation of the mesoporous TiO_2 layer, 0.5 g of TiO_2 (Degussa P25) powder of average size 21 nm was ground in a mortar for 30 min with 2 mL of HNO_3 (pH = 1), 0.1 g carbowax (Sigma Aldrich) and a drop of surfactant. The amount of Ag nanoparticle (10, 20, 30 and 40 μL) of 10 nm particle size purchased from Sigma Aldrich (730785 ALDRICH) was then added separately and grinding was continued for another 5 min. The resulting TiO_2 slurry was spread on top of TiO_2 compact layer using the Doctor Blade method. The electrode was then sintered at 723 K for 30 min and allowed to cool to room temperature. The total thickness of the two TiO_2 layers was ~20 μm. The thickness of the compact and both compact and mesoporous layers was measured using the air wedge method.

In order to adsorb dye molecules, the TiO_2 photoanodes were soaked in anthocyanin sensitizer and ruthenium 535 (N3) dye solution for 24 h. Anthocyanin dye was extracted by immersing 200 g black rice in 200 mL ethanol. N3 dye was dissolved in ethanol to form a concentration of 0.3 mM.

2.4 DSSCs fabrication

In DSSC fabrication the GPE was sandwiched between the dye/TiO_2 photoanode and platinum (Pt) counter electrode. The quasi solid-state DSSC was exposed to 1000 W m^{-2} light illumination at room temperature. The effective area of the test cell was 0.20 cm^2. Autolab potentiostat-galvanostat was used to measure the photocurrent density-voltage (J-V) characteristics of the DSSC. From the J-V plot, the optimum current density, J_{opt} and optimum voltage, V_{opt} at maximum power output were obtained and used in the equation below to calculate the fill factor, FF.

$$FF(\%) = \frac{J_{opt} V_{opt}}{J_{sc} V_{oc}} \times 100\% \tag{2}$$

In Eq. (2), J_{sc} is the short-circuit current density and V_{oc} is the open-circuit voltage. The FF value was then used to calculate the power conversion efficiency (η) of the cell using Eq. (3).

$$\eta(\%) = \frac{J_{sc} V_{oc} FF}{P_{in}} \times 100\% \tag{3}$$

where P_{in} is the total incident power density onto the cell.

2.5 Impedance measurements of DSSC

AUT 85988 advanced electrochemical system (Metrohm Autolab B.V. PGSTAT 128N Netherlands) was used to measure the impedance of the quasi solid-state DSSCs in the frequency range between 10 mHz to 100 kHz under 1000 W m^{-2} light illumination at room

temperature. The potential of each quasi solid-state DSSC was set at their open circuit voltage (V_{oc}), respectively.

2.6 UV-Visible measurement

UV-Visible absorption spectroscopy was carried out from 300 to 1100 nm using the Jasco V-730 spectrophotometer. UV-Visible measurements were performed to study the effect of Ag nanoparticle on TiO_2 photoanode and determine the absorption of photons by anthocyanin sensitizer and N3 dye in the visible spectrum region.

3. Results and discussion

The room temperature ionic conductivities of the series of electrolytes containing different amounts of PEO and PhCh are shown in Fig. 1. The ionic conductivity variation of these electrolytes depends on the synergistic/antagonistic effect between the two polymers [32–34]. Therefore, the highest conductivity was exhibited by the blend with intermediate composition of 70 wt.% PEO and 30 wt.% PhCh. This electrolyte has shown ionic conductivity of 7.36 mS cm^{-1} at room temperature. However, electrolyte containing 80 wt.% and 90 wt.% PEO has poor conductivities compared to other compositions. Samples containing 50 wt.% and 60 wt.% PEO have also shown the conductivity of 6.22 and 6.82 mS cm^{-1}, respectively.
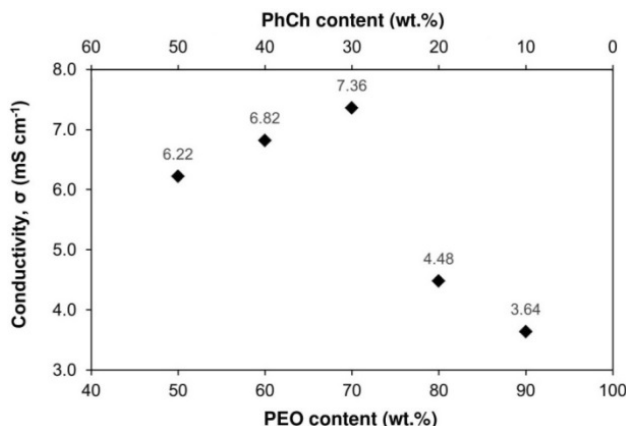

Fig. 1. Ionic conductivity variations with different PEO and PhCh contents in the electrolyte.

The DSSCs have been fabricated using different weight fractions of PEO and PhCh based electrolytes according to the compositions given in Table 1. Cells containing anthocyanin sensitizer were characterized by means of photocurrent density versus cell potential (*J-V*), Fig. 2. Using the *J-V* characteristic curves shown in Fig. 2, the fill factor (*FF*), short-circuit current density (J_{sc}), open-circuit voltage (V_{oc}) and power conversion efficiency (η) were calculated for all the DSSCs and listed in Table 2. The anthocyanin dye sensitizers are not efficient light harvesting agent compared to synthetic dyes, e.g. ruthenium complexes and metal free organic dyes [35–37]. As a result, the efficiencies recorded for these quasi solid-state DSSCs are not very high and need further improvement. Therefore, the highest efficiency solar cell (with S3 electrolyte) was selected to improve the performance further by incorporating Ag nanoparticles in the mesoporous TiO_2. The DSSC containing S3 electrolyte showed energy conversion efficiency of 0.53%. This is the only cell that showed *FF* higher than 0.50 out of the cell series containing anthocyanin.
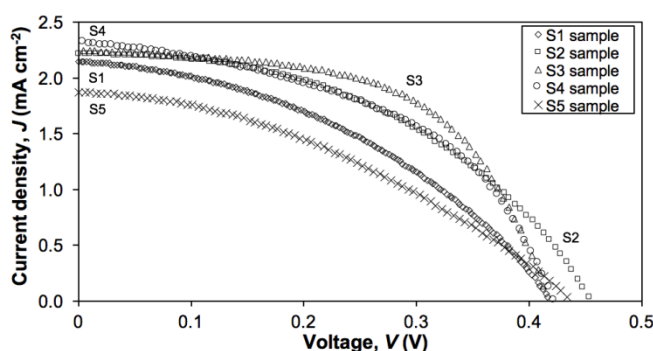
Fig. 2. Current density versus cell potential (*J-V*) curves for DSSCs based on anthocyanin sensitizer and gel polymer electrolytes containing different amounts of PEO and PhCh host polymers. Measurements were taken under light irradiation of 1000 W m^{-2}.

Table 2. The short-circuit current density (J_{sc}), fill factor (*FF*), open-circuit voltage (V_{oc}) and power conversion efficiency (η) of DSSCs based on anthocyanin sensitizer fabricated with gel polymer electrolytes containing different amounts of PEO and PhCh host polymers.

Electrolyte	J_{sc} (mA cm^{-2})	V_{oc} (V)	*FF*	η (%)
S1	2.14	0.43	0.40	0.37
S2	2.21	0.45	0.46	0.46
S3	2.24	0.41	0.58	0.53
S4	2.11	0.43	0.50	0.45
S5	1.87	0.43	0.38	0.31

As mentioned above, the 2nd series of DSSCs were prepared with anthocyanin sensitizer and the mesoporous TiO$_2$ layer incorporated with different amounts of Ag nanoparticles. *J-V* characteristic curves of this series are shown in Fig. 3. The values of *FF*, J_{sc}, V_{oc} and η are given in Table 3. Due to the incorporation of Ag nanoparticles, a significant enhancement of *FF*, J_{sc}, and η is observed. However, the trend of V_{oc} change is not very clear. The effect can be attributed to surface plasmon resonance of incorporated Ag nanoparticles. The collective oscillations of free electrons confined at the surface of the nanoparticles can be induced when the frequency of incident light matches the plasmon frequency of the particles. The collective charge oscillations can generate enhanced electric fields near the surface of nanoparticles, which can facilitate both light absorption as well as charge separation [4, 29–31]. In particular, surface plasmon increases the efficiency by scattering the photons and guiding the waves at the interface [29]. The sample with 10 µL Ag nanoparticles showed 21%, 17.2% and 39.6% increase in J_{sc}, *FF* and η, respectively for anthocyanin based quasi solid-state DSSC.
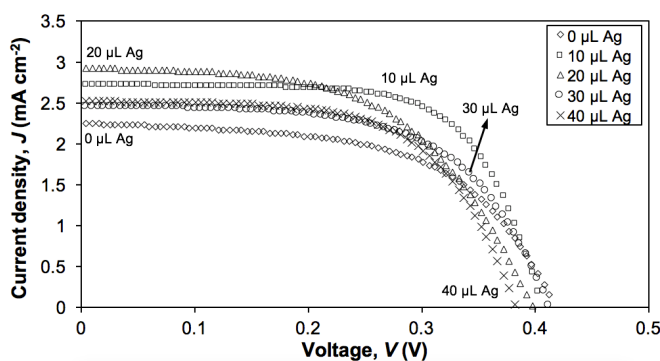

Fig. 3. *J-V* curves for quasi solid-state DSSCs based on anthocyanin sensitizer containing different amounts of Ag nanoparticles in TiO$_2$ photoanode measured under light irradiation of 1000 W m^{-2}.

Table 3. J_{sc}, V_{oc}, FF, and η of DSSCs based on anthocyanin sensitizer containing different amounts of Ag nanoparticles in TiO$_2$ photoanode.

Ag (µL)	J_{sc} (mA cm^{-2})	V_{oc} (V)	FF	η (%)
0	2.24	0.41	0.58	0.53
10	2.71	0.40	0.68	0.74
20	2.92	0.40	0.55	0.64
30	2.45	0.41	0.61	0.61
40	2.52	0.38	0.62	0.59

In addition, the 3rd series of DSSCs were fabricated using N3 sensitizer with electrolytes containing different weight fractions of PEO and PhCh. The *J-V* curves of these cells are shown in Fig. 4 and the *FF*, J_{sc}, V_{oc} and η are tabulated in Table 4. The DSSCs containing N3 dye have shown enhancement of photocurrent compared to that containing anthocyanin since N3 is an efficient light harvesting dye [28]. The highest efficiency for this series is also exhibited by the S3 electrolyte containing cell. The DSSC containing S3 electrolyte showed energy conversion efficiency of 4.61% and J_{sc} of 13.04 mA cm^{-2}. This cell is further studied by incorporating Ag nanoparticles in the mesoporous TiO$_2$ layer.
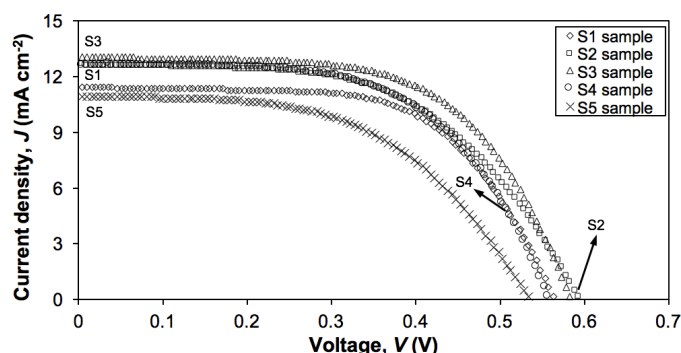
Fig. 4. *J-V* curves for DSSCs based on N3 sensitizer fabricated with GPE containing different weight fractions of PEO and PhCh host polymers under 1000 W m^{-2} light illumination.

Table 4. J_{sc}, V_{oc}, FF, and η of DSSCs based on N3 sensitizer fabricated with GPE containing different weight fractions of PEO and PhCh host polymers.

Electrolyte	J_{sc} (mA cm^{-2})	V_{oc} (V)	FF	η (%)
S1	11.41	0.56	0.62	3.96
S2	12.64	0.59	0.56	4.18
S3	13.04	0.58	0.61	4.61
S4	12.64	0.56	0.58	4.11
S5	10.92	0.53	0.53	3.07

The 4th series of DSSCs were prepared by adding Ag nanoparticles in the TiO$_2$ photoanode of the highest efficiency DSSC with N3 dye and S3 electrolyte. *J-V* characteristic curves for DSSCs with N3 dye containing different amounts of Ag nanoparticles are shown in Fig. 5 and calculated values of *FF*, J_{sc}, V_{oc} and η are given in Table 5. Significant enhancements in *FF*, J_{sc}, and η were observed due to the incorporation of Ag nanoparticles. Since the molar extinction coefficient is higher for N3 dye, the degree of absorption of photons is also higher compared to that of anthocyanin sensitizer [26–28]. Therefore, more photons should be scattered or guided into N3 dye containing cell and thus, more nanoparticles are necessary to be present in the N3 dye containing cell in order to improve the efficiency of DSSCs. Therefore, the highest performance was exhibited by the sample having 20 µL Ag nanparticles. The incorporation of Ag nanoparticles has resulted with 17% and 13%

increase of J_{sc}, and η, respectively. The DSSC containing 20 μL Ag nanoparticles exhibited J_{sc}, V_{oc}, FF and η of 15.24 mA cm^{-2}, 600 mV, 57% and 5.21%, respectively.
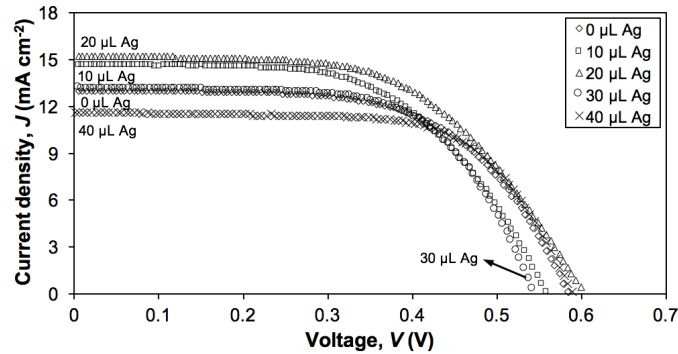

Fig. 5. *J-V* characteristics for quasi solid-state DSSCs with N3 sensitizer and different amounts of Ag nanoparticles in TiO$_2$ photoanode. Measurements were taken under 1000 W m^{-2} light illumination.

Table 5. J_{sc}, V_{oc}, FF, and η of DSSCs with N3 sensitizer containing different amounts of Ag nanoparticles in TiO$_2$ photoanode.

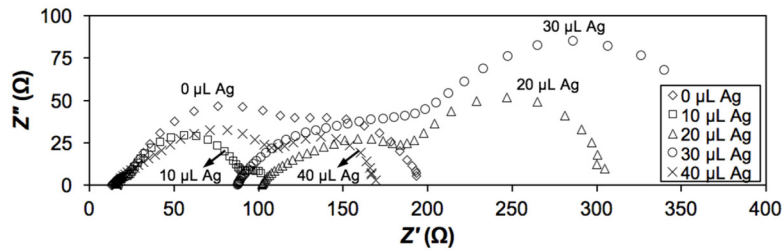| Ag (μL)	J_{sc} (mA cm^{-2})	V_{oc} (V)	FF	η (%)
0	13.04	0.58	0.61	4.61
10	14.74	0.56	0.57	4.71
20	15.24	0.60	0.57	5.21
30	13.16	0.55	0.64	4.63
40	11.66	0.59	0.66	4.54

Fig. 6. EIS for quasi solid state DSSC with anthocyanin sensitizer and different amounts of Ag nanoparticles in TiO$_2$ photoanode.

Figure 6 shows the Nyquist plots of the DSSCs using anthocyanin dye fabricated with TiO$_2$ photoanode containing different amounts of Ag nanoparticles. The electrochemical impedance spectroscopy (EIS) was used to investigate the charge transport behavior in DSSCs with different amounts of Ag nanoparticles in TiO$_2$ photoanode. It is common to observe three semicircles in the impedance spectroscopy obtained under applied biasing conditions. The impedance plots given in Fig. 6 also showed the existence of three semicircles. Therefore, the results can be interpreted by the equivalent circuit given in Fig. 7(a) corresponding to the Nyquist plot given in Fig. 7(b). Consequently, it can be proven that the real (Z') and imaginary (Z'') parts of the DSSC impedance are given as below:

$$Z' = R_s + \left[\sum_{i=1}^{3} \frac{R_i + R_i^2 k_i^{-1} \omega^{p_i} \cos\left(\frac{\pi p_i}{2}\right)}{1 + 2R_i k_i^{-1} \omega^{p_i} \cos\left(\frac{\pi p_i}{2}\right) + R_i^2 k_i^{-2} \omega^{2 p_i}} \right] \tag{4}$$

$$Z'' = \sum_{i=1}^{3} \frac{R_i^2 k_i^{-1} \omega^{p_i} \sin\left(\dfrac{\pi p_i}{2}\right)}{1 + 2R_i k_i^{-1} \omega^{p_i} \cos\left(\dfrac{\pi p_i}{2}\right) + R_i^2 k_i^{-2} \omega^{2p_i}} \tag{5}$$

Here, R_s is ohmic serial resistance, R_1 is charge transfer resistance at the Pt counter electrode, R_2 is charge transfer resistance at the TiO_2/dye/electrolyte interface and R_3 is ionic diffusion resistance in the electrolyte [38]. k_1^{-1}, k_2^{-1} and k_3^{-1} are leaky capacitors or constant phase elements (CPEs) at Pt counter electrode/electrolyte interface, TiO_2/dye/electrolyte interface and electrolyte, respectively [38]. p_i is the right angle ratio ($0 < p_i < 1$) between the diameter of the depressed semicircle and the vertical axis [39]. The calculated R_s, R_1, R_2, and R_3 values are listed in Table 6 for the DSSCs with anthocyanin sensitizer and different amounts of Ag nanoparticles in TiO_2 photoanode.
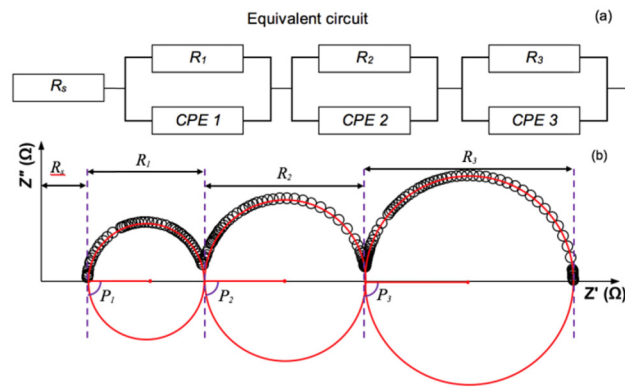

Fig. 7. (a) The equivalent circuit and (b) respective Nyquist plots used in the present study to represent DSSCs.

Table 6. R_s, R_1, R_2, R_3 values for quasi solid-state DSSCs based on anthocyanin sensitizer with different amounts of Ag nanoparticles in TiO_2 photoanode.

Ag (µL)	R_s (Ω)	R_1 (Ω)	R_2 (Ω)	R_3 (Ω)
0	13.5	12.0	97.0	70.0
10	15.2	11.0	62.5	18.0
20	102.0	22.0	65.0	118.0
30	88.0	42.0	71.0	180.0
40	16.3	18.0	75.5	59.0

The arc in the middle frequency range, 1-1000 Hz represents the charge transfer resistance (R_2) between the dye-adsorbed photoanode and electrolyte interface [40–42]. The charge transport resistance is affecting the overall DSSC performance of the cell and thus as expected, the lowest charge transfer resistance is given by highest efficiency DSSC. The efficiency and $1/R_2$ (charge transport conductance) is plotted against the Ag nanoparticle content and shown in Fig. 9 in order to understand the influence of the charge transport resistance to the performance of the DSSC with anthocyanin (circular symbols) and N3 dyes (square symbols). The maximum efficiency and maximum charge transport conductance between the dye-adsorbed photoanode and electrolyte interface is shown for 10 µL Ag content in TiO_2 photoanode for the cells with anthocyanin dye. This concludes the contribution of Ag nanoparticles towards the enhancement in the charge transport and resulted improvement in cell efficiency.
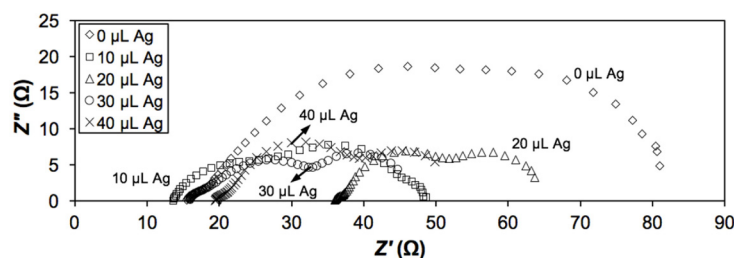
Fig. 8. EIS for quasi solid-state DSSC with N3 sensitizer fabricated and TiO_2 photoanode containing different amounts of Ag nanoparticles.

Table 7. R_s, R_1, R_2, R_3 values for quasi-solid state DSSCs with N3 sensitizer and TiO_2 photoanode containing different amounts of Ag nanoparticles.

Ag (µL)	R_s (Ω)	R_1 (Ω)	R_2 (Ω)	R_3 (Ω)
0	15.1	5.0	39.0	24.0
10	13.6	14.2	17.1	4.0
20	35.8	2.0	14.2	12.8
30	15.8	2.7	14.9	13.1
40	19.4	2.8	16.4	14.7

Figure 8 shows the Nyquist plots of the DSSCs with N3 dye and different amounts of Ag nanoparticles in TiO_2 photoanode. The impedance plots given in Fig. 8 also show a trend of having three semicircles. R_s, R_1, R_2, and R_3 values calculated for the DSSCs prepared with N3 sensitizer and different amounts of Ag nanoparticles are tabulated in Table 7. As expected, the charge transport resistance R_2 is lower for the cell with N3 dye compared to that with anthocyanin sensitizer. However, with added Ag nanoparticles, a significant drop in R_2 is observed. As seen from Fig. 9, both the maximum efficiency and charge transfer conductance are given by DSSCs with N3 dye containing 20 µL Ag content in TiO_2 photoanode.
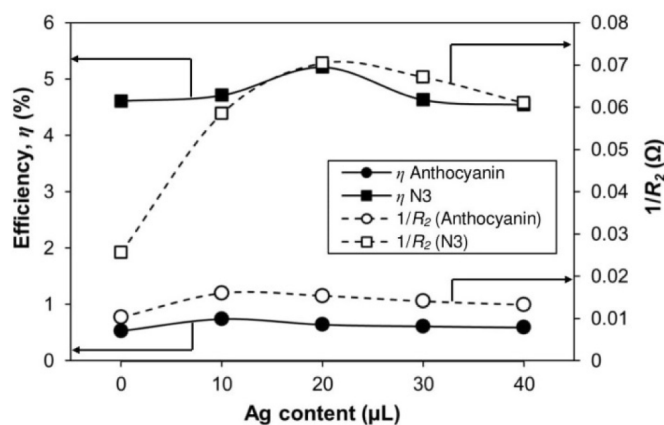

Fig. 9. The efficiency and $1/R_2$ (charge transport conductance) against the Ag nanoparticle content in TiO_2 photoanode of DSSC. Circular symbols and square symbols represent anthocyanin and N3 sensitizers, respectively. Filled and unfiled symbols give efficiency and charge transport conductance ($1/R_2$), respectively.

Incorporated Ag nanoparticles contribute to performance by improving charge transport and also by acting as light scattering centers [40–42]. It is well known that N3 dye is an efficient light harvesting sensitizer than anthocyanin. Therefore, N3 can harvest more photons than anthocyanin, thus more light should be scattered for N3 sensitizer to get higher photocurrent. This may be the reason for showing the maximum efficiency at higher nanoparticle content for N3 compared to anthocyanin sensitizer.

The *J–V* plot of DSSCs can be represented by the equivalent circuit as shown in Fig. 10 [43]. In Fig. 10, I_{ph} is the ideal photocurrent, C_1 is a capacitive element and R_{sh} is the shunt resistance. The sum of charge transfer resistance at Pt/FTO interface (R_1), diffusion of redox couple (R_2) and ohmic serial resistance (R_3) make the series resistance, R_s. R_{sh} and R_s control the *FF* of DSSC. Higher R_{sh} and/or lower R_s can increase/decrease the *FF*, thus the efficiency of DSSC may increase. Table 8 lists the values of R_s and R_{sh} for DSSC based anthocyanin and N3 sensitizer with different amounts of Ag nanoparticles in TiO$_2$ photoanode.
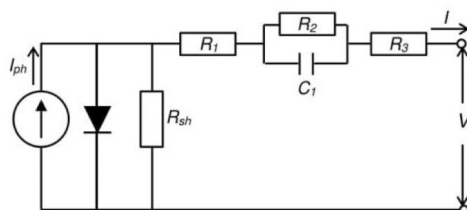

Fig. 10. Equivalent circuit based on *J–V* characteristics of DSSC.

Table 8. Values of series resistance (R_s) and shunt resistance (R_{sh}) for DSSC with anthocyanin and N3 sensitizer and different amounts of Ag nanoparticles in TiO$_2$ photoanode.

Ag (µL)	Anthocyanin		N3 dye	
	R_s (Ω)	R_{sh} (kΩ)	R_s (Ω)	R_{sh} (kΩ)
0	204.28	7.69	54.12	5.67
10	132.47	25.80	55.56	5.96
20	205.07	14.33	64.33	8.67
30	175.49	13.76	48.10	5.45
40	163.32	12.04	47.48	5.33

From Table 8, it can be seen that the R_{sh} value of DSSC with anthocyanin and TiO$_2$ containing 10 µL Ag nanoparticle and DSSC with N3 dye and TiO$_2$ containing 20 µL Ag nanoparticle are the highest. It is reported that the value of R_{sh} should be high so that it can improve the fill factor for high solar efficiency [43]. Based on this work, the trend of solar efficiency obtained for DSSC with anthocyanin and N3 dye containing different amounts of Ag nanoparticles is similar to the trend of R_{sh} and Ag nanoparticle content as shown in Table 8.

Figure 11(a) shows the UV–Vis absorption spectra of TiO$_2$ layer containing different amounts of Ag nanoparticles. Based on Beer–Lambert's law [44] given below, the energy gap, E_g of TiO$_2$ can be calculated.

$$\alpha(\lambda)\frac{hc}{\lambda} = B\left(\frac{hc}{\lambda} - E_g\right) \tag{6}$$

Here α is the absorption coefficient of incident photon energy, hc/λ is the incident photon energy and B is a constant. α depends on thickness of TiO$_2$. Ghobadi [44] has rearranged Eq. (6) in order to determine E_g and is given as below:

$$\left(\frac{\text{Abs}(\lambda)\times hc}{\lambda}\right)^2 = B_1\left(\frac{hc}{\lambda} - E_g\right) + B_2 \tag{7}$$

In Eq. (7) above, B_1 and B_2 are constants. Figure 11(b) shows a plot of $\left(\dfrac{\text{Abs}(\lambda) \times hc}{\lambda}\right)^2$ against $\dfrac{hc}{\lambda}$ using the data obtained in Fig. 11(a). A straight line that cuts the x-axis gives the E_g value of TiO$_2$ containing different amounts of Ag nanoparticle and the values are listed in Table 9. It can be seen that addition of Ag nanoparticle up to 20 µL decreased the E_g of TiO$_2$ from 2.78 eV to 2.70 eV. This implied that the presence of Ag nanoparticles have downshifted the Fermi level of TiO$_2$ towards the valence band. As a result, the driving force for electron injection from dye excited state to TiO$_2$ conduction band is increased. Wei et. al [45] reported that the charge quantity in the conduction band of 1.2 atomic% Ag nanoparticle in TiO$_2$ is larger than that of TiO$_2$ without Ag nanoparticle. This inferred that the addition of 20 µL Ag nanoparticle in TiO$_2$ have increased the TiO$_2$ (e$^-$) concentration in conduction band and increased J_{sc} of the DSSC. From Fig. 11(a), the addition of more than 20 µL Ag nanoparticles in TiO$_2$ can results in the oxidation of the metal nanoparticle from Ag to Ag$^+$. This can also increase the recombination rate that could led to a reduction in electron concentration in the conduction band of TiO$_2$ [45]. The decrease electron density in TiO$_2$ conduction band shifted the Fermi level of TiO$_2$ away from the valence band. This reduced the driving force of electron injection from dye excited state to TiO$_2$ conduction band. Hence, the J_{sc} of DSSC will decreased. This is in line with the E_g gap value shown in Table 9 for Ag nanoparticle content greater than 20 µL. Decrease in J_{sc} and photon-to-current efficiency beyond 20 µL Ag nanoparticles can also result in a loss of absorbing dye volume due to the large volume of Ag nanoparticle. In addition, aggregation of Ag nanoparticle may also occurs resulting in electron trapping [46–48] This processes would diminish the electron density thus decreasing J_{sc}.
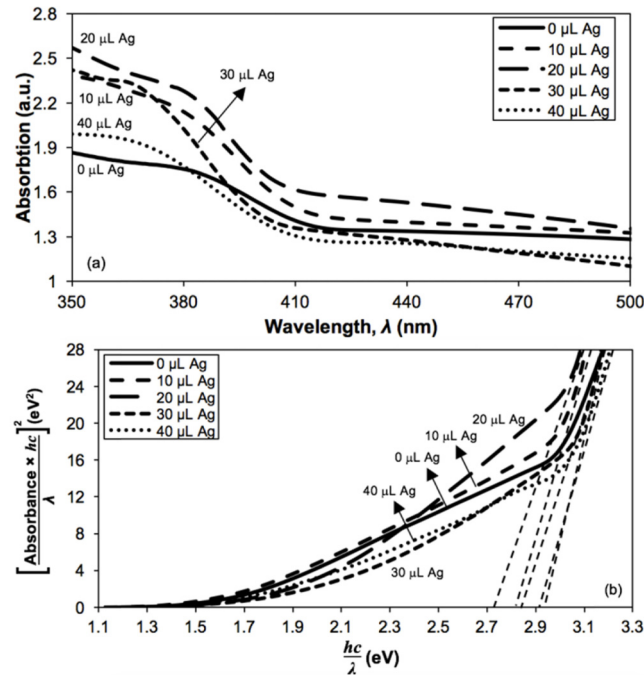

Fig. 11. (a) UV-Vis absorption spectra and (b) $\left(\dfrac{\text{Abs}(\lambda) \times hc}{\lambda}\right)^2$ against $\dfrac{hc}{\lambda}$ plot of TiO$_2$ layer containing different Ag nanoparticles composition.

Table 9. Energy gap of TiO$_2$ layer containing different amount of Ag nanoparticles obtained from Fig. 10(b.)

Ag (µL)	E_g (eV)
0	2.78
10	2.76
20	2.70
30	2.89
40	2.92

Figure 12 shows the UV-Visible plot of TiO$_2$ containing different amounts of Ag nanoparticle soaked in anthocyanin sensitizer. It can be seen that TiO$_2$/Ag photoanode with 20 µL Ag nanoparticles has higher absorption inferring that more photons were absorbed by anthocyanin due to the plasmonic effect. The downshift of TiO$_2$ Fermi level to a more positive potential has increased the driving force of electron injection from anthocyanin sensitizer excited state to TiO$_2$ conduction band. The same pattern was observed in the J_{sc} values of DSSC with anthocyanin sensitizer containing 20 µL Ag nanoparticles in TiO$_2$ photoanode where this device exhibited highest J_{sc} values as shown in Table 3. The increase in J_{sc} for DSSC with 0 µL Ag nanoparticle and with 20 µL Ag nanoparticle is 30%.
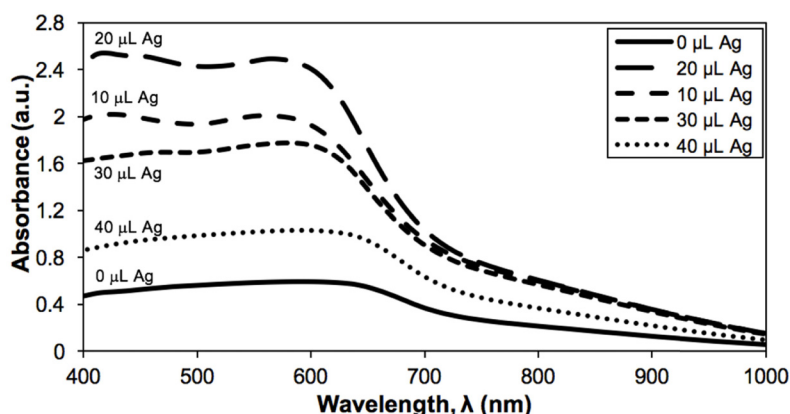

Fig. 12. UV-Vis absorption spectra of TiO$_2$ layer containing different Ag nanoparticles soaked in anthocyanin sensitizer.

Figure 13 shows the UV-Visible plot of TiO$_2$ containing different amount of Ag nanoparticle soaked in N3 dye. It can be seen that TiO$_2$/Ag photoanode with 20 µL Ag nanoparticles has the highest absorption. This implied that more photon was absorbed by N3 dye due to the addition of Ag nanoparticle with TiO$_2$. The downshift of TiO$_2$ Fermi level has increased the driving force of electron injection from N3 dye excited state to TiO$_2$ conduction band. The same pattern was observed in the J_{sc} values of DSSC with N3 sensitizer containing 20 µL Ag nanoparticles in TiO$_2$ photoanode where this device exhibited the highest J_{sc} value as shown in Table 5. Based on this work, it has been shown that plasmonic effect of Ag nanoparticles in TiO$_2$ improved the absorption of photon and the performance of DSSC.
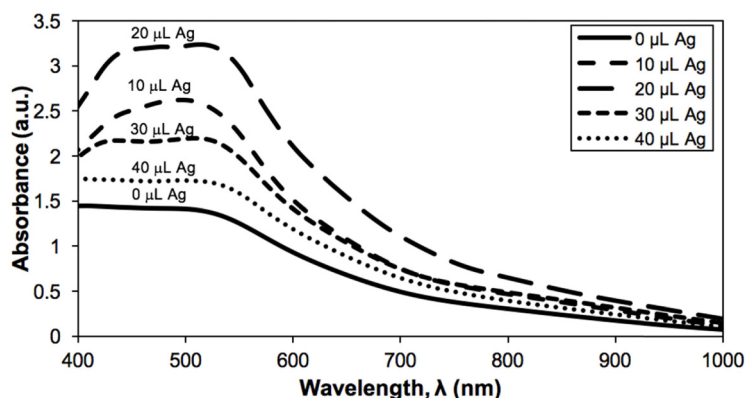
Fig. 13. UV-Vis absorption spectra of TiO_2 layer containing different Ag nanoparticles soaked in N3 dye.

4. Conclusions

The study of ionic conductivity in gel polymer electrolytes (GPEs) containing different weight fractions of PEO and PhCh revealed that the highest conductivity is given by the blend of 70 wt.% PEO:30 wt.% PhCh. This composition showed ionic conductivity of 7.36 mS cm^{-1} at room temperature. The electrolytes containing 80 wt.% and 90 wt.% PEO has poor conductivities compared to other compositions. Samples containing 50 wt.% and 60 wt.% PEO containing samples also exhibited a conductivity of 6.22 and 6.82 mS cm^{-1}, respectively. DSSCs fabricated with GPE containing 70 wt.% PEO:30 wt.% PhCh revealed the highest solar conversion efficiency for both anthocyanin sensitizer and N3 dyes. Therefore, the efficiencies of these cells are governed by ionic conductivity of the electrolytes.

The performance of DSSCs with anthocyanin sensitizer and N3 dye were improved by adding Ag nanoparticles in TiO_2 photoanode. The cell fabricated with TiO_2 photoanode containing 10 µL Ag nanoparticles showed 21%, 17.2% and 39.6% increase in J_{sc}, FF and η, respectively for quasi solid-state DSSC soaked in anthocyanin with respect to DSSC with photoanode that does not contains Ag nanoparticles.

The DSSCs with N3 dye have shown a dramatic enhancement of photocurrent compared to that of DSSC with anthocyanin sensitizer. The DSSC containing 70 wt.% PEO:30 wt.% PhCh electrolyte showed energy conversion efficiency of 4.61% and J_{sc} of 13.04 mA cm^{-2}. The DSSC with 20 µL Ag nanoparticles in TiO_2 photoanode exhibited J_{sc}, V_{oc}, FF and η of 15.24 mA cm^{-2}, 600 mV, 57% and 5.21%, respectively. The incorporation of Ag nanoparticles resulted in 17% and 13% increase in J_{sc}, and η, respectively for cells with N3 dye. The performance enhancement with added Ag nanoparticles can be attributed to improvement of light scattering and charge transport due to plasmonic resonance.